Single-step soft-imprinted large-area nanopatterned anti-reflection coating

Jorik van de Groep,[1] Pierpaolo Spinelli,[1,2] and Albert Polman[,1]*

[1] Center for Nanophotonics, FOM Institute AMOLF, Science Park 104, 1098 XG Amsterdam, The Netherlands

[2] Energy Research Center of the Netherlands ECN, Westerduinweg 3, 1755 LE Petten, The Netherlands

ABSTRACT:

We demonstrate an effective nanopatterned anti-reflection coating on glass that is based on sol-gel chemistry and large-area substrate-conformal soft-imprint technology. The printed 120 nm tall silica nanocilinders with a diameter of 245 nm in a square array with 325 nm pitch, form an effective-index (n = 1.20) anti-reflection coating that reduces the double-sided reflection from a borosilicate glass slide from 7.4% to 0.57% (averaged over the visible spectral range) with a minimum reflectance < 0.05% at 590 nm. The nano-glass coating is made using a simple process involving only spin-coating and an imprint step, without vacuum technology or annealing required. The refractive index of the nano-glass layers can be tailored over a broad range by controlling the geometry ($1.002 < n < 1.44$ in theory), covering a wide range that is not achievable with natural materials. We demonstrate that the nano-glass coating effectively eliminates glare from smart-phone display windows and significantly improves the efficiency of glass-encapsulated solar cells. These features, that are achieved over an angular range as wide as ±50°, together with strong hydrophobicity and mechanical durability, make nano-glass coatings a promising technology to improve the functionality of optoelectronic devices based on glass encapsulation.

KEYWORDS: anti-reflection coating, nanoimprint lithography, nanopattern, hydrophobicity

Light that impinges on the interface between two materials with different refractive indices exhibits reflection. In many applications, such reflection losses are unwanted. For example, reflection losses at the air/glass interface reduce the efficiency of photovoltaic modules,[1] and the glare of reflected sunlight off the screen of mobile electronic devices reduces the visibility of the screen. Anti-reflection (AR) coatings, optically thin (dielectric) layers with carefully chosen refractive index and thickness, can minimize these reflection losses through interference effects. An optimized AR coating for material with index n in air has a refractive index $\sqrt{n}$ and an optical thickness $t = \lambda/4\sqrt{n}$, where λ is the free-space wavelength for which the AR effect is optimized.

While such AR interference coatings are commonly used for high-index materials, such as for example silicon solar cells,[2] applying such coatings on glass ($n \approx 1.5$) is difficult, as no material is readily available in nature with a refractive index $n = \sqrt{1.5} = 1.22$. Alkali halides such as MgF ($n = 1.38$) and LiF ($n = 1.39$) have refractive index lower than glass,[3] but are still far from ideal. Lower refractive indices can be obtained using sub-wavelength structuring of materials. For example, porous materials can have indices lower than that of the constituent bulk materials.[4-7] However, such coatings are often randomly structured, and therefore offer limited control over the index. As a result, such layers often lack large-scale uniformity and do not provide the theoretically achievable minimum reflection.

Directional scattering of resonant nanostructures has also been used to form efficient AR coatings,[8, 9] however such coatings require high-refractive index nanostructures and have a bandwidth limited by the resonance line width. Alternatively, tapered sub-wavelength

nanostructures can be used to create a “graded index” material, giving rise to a gradual change in refractive index rather than a sudden one.[10-15] Although the graded-index AR coatings are inherently more broadband than interference AR coatings, they often require complex fabrication schemes and are often composed of fragile high-aspect-ratio surface geometries.

AR coatings for glass substrates have been demonstrated using colloidal self-assembly[16] and lithography,[15-17] porous silica solgels,[4-7] sputtering,[18] anodic aluminum oxide formation,[19] laser interference-lithography[13] and nanoimprint lithography.[10, 11, 14, 15] A disadvantage of many of the techniques mentioned above is that they often require complex (many-step) fabrication procedures,[10-15, 18] provide limited control over pattern spatial homogeneity and reproducibility,[5-7, 16, 17, 19] and are not substrate conformal.[12] On the other hand, the more simple fabrication schemes yield relatively poor performance and/or uniformity.[5, 16, 17, 19] The combination of high performance anti-reflection properties, accurate control over nanoscale geometry, and facile fabrication procedure has so far not been realized.

Here, we use substrate-conformal imprint lithography (SCIL)[20] to demonstrate an interference-based AR coating that: 1) is simple to fabricate using a single-step process; 2) allows for large-area cost-effective fabrication with large-area uniformity; 3) is substrate conformal, thereby allowing printing on rough surfaces; 4) exhibits reflectance equal to the theoretical minimum for AR coatings. Further advantage is that the method is easily optimized for specific applications (i.e. different types of substrate materials); and that the printed AR coating is strongly hydrophobic. This prevents scattering losses due to accumulation of water droplets, and makes the surface self-cleaning. Our SCIL-based AR coating fabrication method requires no external

pressure,[10-12] no elevated temperatures,[6, 11-15] no sacrificial layers,[13, 14] no UV-irradiation,[10] no etching[7, 12, 13, 15, 16] or other vacuum techniques,[13, 18, 19] and exhibits excellent large-range homogeneity and reproducibility.[5-7, 10-12, 15-17, 19]

The AR coating is fabricated out of liquid-silica solgel, which is based on the liquid alkoxide tetra-methyl-ortho-silicate (TMOS), $Si(OCH_3)_4$.[20] After hydrolysis, this precursor yields methanol and silicon hydroxyl $(CH_3O)_3Si\text{-}OH$, which can subsequently condensate into stable Si-O-Si bonds to form silica. Accurate control over the degree and rate of condensation is essential to prevent porosity and thereby the formation of stress-induced cracks in the solidified nanopatterned coating. Partial substitution of TMOS by the organic alkoxide methyl-tri-methoxy-silane (MTMS), $CH_3\text{-}Si(OCH_3)_3$, provides control over the degree of cross linking. This allows the formation of gels with a higher concentration of silicon precursors, and thereby results in a less porous material and less shrinkage. Furthermore, cured MTMS layers are optically transparent and its methyl group makes the resulting solgel layer hydrophobic.

To start the solgel fabrication,[20] 7.1 grams of MTMS is mixed with 7.93 grams of TMOS in a polypropylene jar (250 mL). Next, 3 grams of 1-propanol is added to increase the mixability with water, followed by 6.6 grams of 1M formic acid in water. Next, the temperature of the mixture is controlled by an external water bath and the mixture is left to react at 36 °C for 120 min. After this, 10.3 grams of water is added, as well as 92.4 grams of 1-propanol to dilute the hydrolysis mixture. The mixture is left at room temperature for 30 min, and subsequently stored at -25 °C. Next, the imprint resist is fabricated from this mixture by adding a dilution mixture consisting

out of 7.64 grams of 2-ethoxy-ethyl ether, 20.63 grams of water, and 99.06 grams of 1-propanol. The final imprint resist is stored at least 16 hours at -25 °C before use.

The AR coating fabrication process consists of a single imprint procedure in which the substrate is spin coated (800 rpm, 10 s) with a 90 nm thick layer of the silica-based solgel, into which a nanopatterned PDMS stamp is subsequently applied (Fig. 1a). Capillary forces pull the stamp into the solgel, creating a substrate-conformal imprint. After 30 minutes of drying in ambient conditions, the solgel has solidified and the stamp can be reused thousands of times.[20] The resulting silica nanostructures are dielectric and exhibit no optical absorption throughout the entire visible spectral range, as confirmed with spectroscopic ellipsometry (see S1). The imprinted silica nanopattern is sub-wavelength and designed such that the effective index of the coating corresponds to the theoretical optimum for an interference AR coating on glass.

The pattern is composed of a square array of silica nanocylinders. The array pitch is 325 nm, such that no diffraction of free-space light occurs in the visible spectral range. Figure 1b shows a scanning electron microscope (SEM) image of an array of silica cylinders printed onto a silicon substrate, showing the cylindrical shape of the nanoparticles. A thin flat residual layer of solgel is clearly visible below the particles and is measured to be 30 nm thick. The particles are slightly tapered, with diameters of ~225 and ~260 nm at the top and bottom, respectively. The large-scale uniformity of the printed pattern is clearly visible in Fig. 1c. The height of the particles was measured to be 120 nm using atomic force microscopy (inset Fig. 1c).

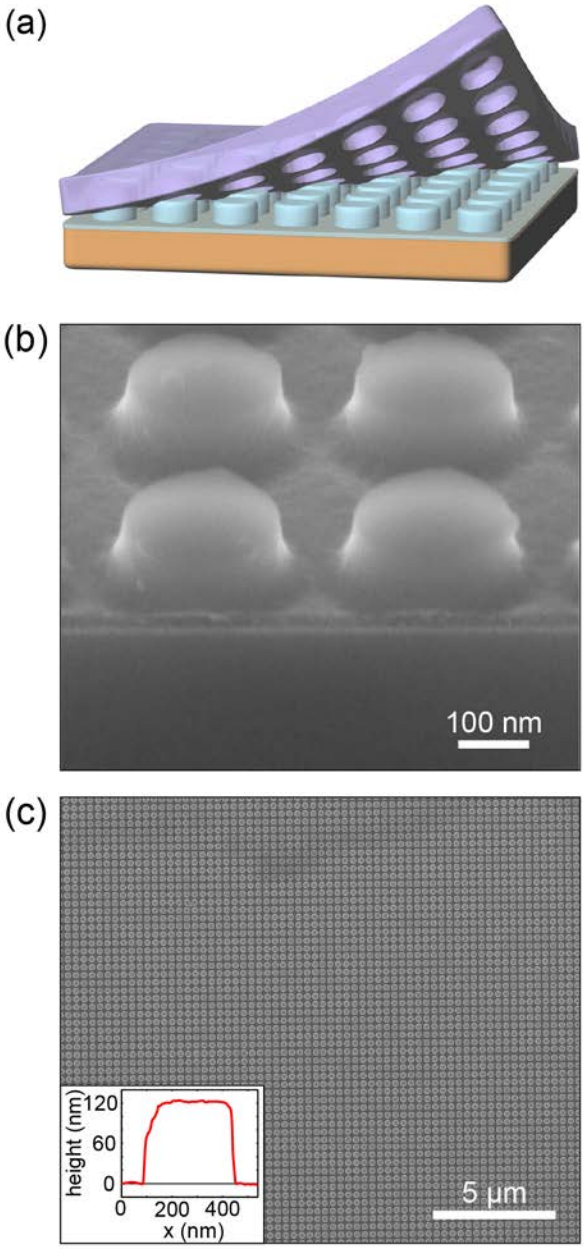

Figure 1. (a) Schematic of the one-step nanoimprint lithography fabrication method. The spin-coated solgel is patterned by a PDMS stamp to create an effective-index AR coating. (b) SEM image of the solgel nanocylinder array on a Si substrate, showing the cylindrical shape of the nanoparticles and the 30 nm residual solgel layer (cleaved sample imaged under 52°). (c) SEM image showing the large-scale uniformity. A line trace of an AFM scan is shown as an inset.

Next, borosilicate microscope slides (24 × 24 × 1 mm, SCHOTT AG, refractive index $n = 1.485$ as retrieved from reflection measurements) were cleaned (base piranha and O_2 descum plasma) and patterned. Samples were coated at the front only, or at the front and the rear. When patterning the rear side of the glass, the front is protected during processing by coating the pattern with a thick layer of S1813 photo resist (2000 rpm, 32 s). After patterning the rear, the protective layer is easily removed by rinsing in acetone. An integrating sphere optical setup was used to measure the total reflectance of a flat reference substrate, and one- and two-side coated glass substrates (see S2 for schematic). A white supercontinuum laser (Fianium SC400-4, unpolarized) was used as a light source, attenuated using the reflection of a glass wedge and a neutral density filter (ND3.0). The samples were mounted at the back of an integrating sphere (LabSphere) with an 8° angle of incidence to prevent the specular reflection from escaping through the sphere entrance. A 105-µm-core collection fiber (Thorlabs, FG105 UCA, NA=0.22) directs the light to a spectrograph (Acton SpectraPro 2300i) and a Si CCD camera (Pixis 400). Spectra are measured over two spectral ranges (420 – 800 nm and 800 – 1000 nm) using two different gratings (150 lines/mm, blazed for 500 nm and 800 nm). Each spectrum is the result of 100 accumulations of 250 ms integration time. A 15-point moving average (6 nm bandwidth) is used to smoothen out experimental noise. A silver mirror (Thorlabs PF10-03-P01) is used for a reference reflection measurement, taking into account the specified reflection for the mirror (see S2). For the patterned substrates, the spectra shown are the average of the spectra measured on the front and rear sides.

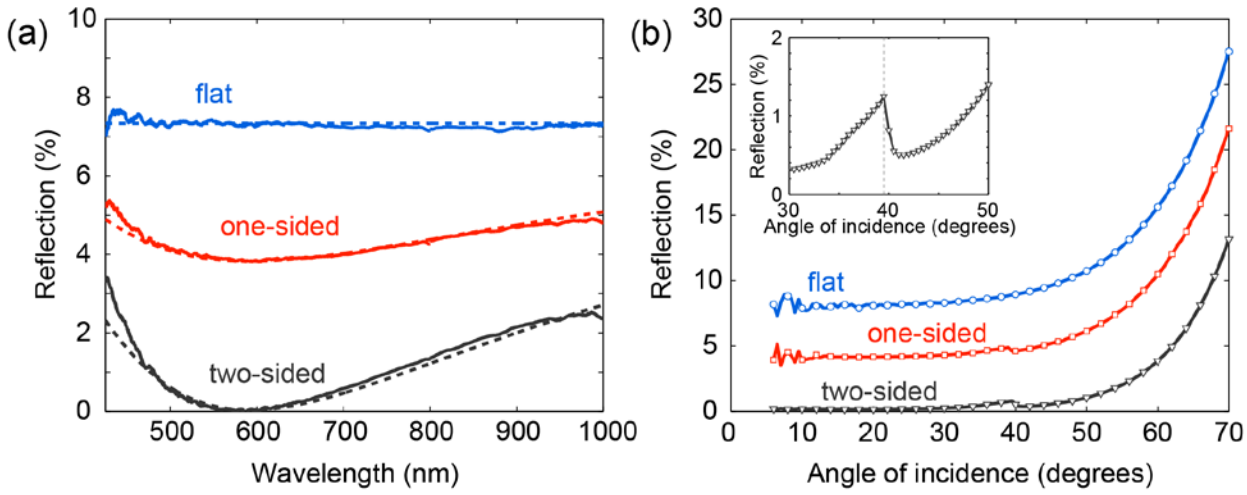

Figure 2. (a) Measured total reflection spectra for a flat reference (blue), and one-side patterned (red), and two-side patterned (black) glass substrates. The dashed lines show the calculated reflection. (b) Measured specular reflection as a function of angle of incidence for the same samples (λ = 532 nm, averaged over s- and p-polarization). A high-resolution plot of the angular response of the two-side patterned substrate around 40 degrees is shown as an inset (s-polarization).

The nanostructured AR coating causes a strong broadband reduction in reflection (Fig. 2a). For both the one- and two-sided substrate, a clear minimum in reflection can be observed around λ = 590 nm as a result of the interference-induced anti-reflection effect. The reflection at λ = 590 nm is reduced from 7.3 % to 3.8 % by patterning one side of the substrate, and further reduced to < 0.05% (the measurement error) when both sides are patterned. The low reflection minimum indicates that the effective index of the AR nanopatterned layer is very close to the optimal value of n = 1.22. We calculate the average reflectance (weighted for the AM1.5 solar spectrum intensity) over spectral bands relevant for display applications (e.g. for outside use) and solar panels based on Si solar cells. For display applications (phone screens, tablets, etc.), only the spectral range up to λ = 700 nm is relevant due to the sensitivity of the human eye,[21] whereas

for solar applications the full measured spectral range is relevant. The results are shown in Table 1, showing an average reflectance of 0.57 % in the visible spectral range and 0.97 % for the full spectral range.

Reflectance (%)	**Display applications**	**Solar applications**
Flat	7.35	7.30
One-side coated	4.10	4.24
Two-side coated	0.57	0.97

Table 1. AM1.5 averaged reflectance for display (425 – 700 nm) and solar (425 – 1000 nm) applications for flat, one-side and two-side coated borosilicate glass.

Finally, haze (random scattering of light) induced by the nanopattern AR coating should be minimized for display applications. The design of our nanopattern coating as an effective index AR coating does not distort the plane-wave nature of light propagating through the nanparticle layer (see S3). As a result, the nanopattern AR coating exhibits extremely low haze in the visible spectral range (see S4 for photograph).

Note that the wavelength of the 0% reflection dip can be tuned by varying the height of the nanocylinders, to match a specific application. For example, slightly lower nanoparticles will blue-shift the interference dip and further minimize the average reflectance for display applications. Furthermore, the size of the nanoparticle can be tuned to obtain a different effective index that can be optimized for substrates with different index. Assuming a minimum particle/hole diameter of 20 nm as the limiting resolution of SCIL, the effective index can in theory be tuned in the range n_{eff} = 1.001 – 1.439, providing efficient AR coatings for substrates

with index in the range n = 1.002 – 2.070. Our coating thus allows full tunability according to the application and substrate used.

To demonstrate that the anti-reflection properties of the nanopatterned surface are the result of the effective index experienced by the light, we performed transfer-matrix calculations using Fresnel equations and an effective index for the nanopattern layer. We neglect the tapered side walls and approximate the shape of the nanoparticles as prefect cylinders with d = 245 nm and h = 120 nm. Using a 325 nm pitch and refractive index for the solidified solgel n_{solgel} = 1.44 (see Fig. S1), the volume-averaged effective index is calculated to be n_{eff} = 1.20, very close to optimum of 1.22. Note that for sub-wavelength structures with an index close to 1.5, this simple geometrical average is a very good approximation to more advanced effective medium calculations,[22] such as the Maxwell-Garnett and Bruggeman theories.[23, 24] The calculations take into account the 30 nm thick residual layer and the angle of incidence of 8°. We calculate the coherent reflection and transmission coefficients of both interfaces separately, and use the fact that the substrate is thick in order to treat the interaction between the front and back interfaces of the glass incoherently. Using an infinite geometric progression we take into account the infinite number of reflections between the top and bottom interface and average over both polarizations.

The results for all three interfaces show very good correspondence with the measurements (Fig. 2a). Both the trends and absolute reflections are well reproduced by the calculations, confirming that the AR coating can be described by an effective medium (see also Fig. S3a for simulated field and phase profiles). Note that for both the one- and two-sided substrates, a clear discrepancy between measurement and calculation is observed for λ < 500 nm. We attribute this

to light that is diffracted into the substrate and then coupled out again. Although the 325 nm pitch is small enough to prevent diffraction in free space, diffraction in the substrate can occur when $\lambda \leq 527$ nm (for 8° angle of incidence). Since the diffraction angle lies above the critical angle of a glass-air interface, this light is trapped in guided modes until it couples back out through the reverse process, thereby contributing to reflection and transmittance. Such mode coupling is not captured by the effective medium calculations, hence the discrepancy. Note that in many applications the glass is in optical contact with another medium on the rear, such that this interface will not give rise to total internal reflection in the glass, eliminating the increase in reflection. Alternatively, decreasing the pitch to 250 nm, which is well possible with the SCIL technique, will eliminate diffraction effects in the visible spectral range altogether (see S3 for FDTD simulations).

We measured the angle-dependent specular reflection using a dual rotation stage (Huber) to control the angle of incidence θ between 6 – 70° in steps of 0.5°. A λ = 532 nm diode laser (WiTec), polarization-maintaining single-mode fiber (WiTec) and outcoupler (Thorlabs CFC-8X-A) were used to illuminate the samples with ~20 mW of polarized light (300:1 s/p polarization ratio). The polarization was controlled with the outcoupler orientation and analyzed with a polarizer. The reflected light was sent through a diffuser (Thorlabs DG10-1500-MD) mounted in front of a calibrated power meter (Thorlabs PM300) in order to illuminate the detector surface uniformly. For each angle of incidence, the mean of 100 power measurements was recorded.

The polarization-averaged angle-resolved reflectance is shown in Fig. 2b (see Fig. S5 for polarization-resolved data). The nanopattern reduces the reflectance for the entire measured angular range. The two-side coated substrate has a reflectance < 1 % for angles up to 50°. Comparing the reflection at 50° with that at 10° shows that the nanopattern reduces the angular sensitivity. The absolute increase in reflectance over this angular range is 2.8% for the flat substrate, whereas it is reduced to 2.2% and only 0.9% for the one- and two-sided substrates respectively. Such low angular sensitivity is of major importance for stationary photovoltaic modules, for which reflection off the front glass plate at large angles of incidence reduces the annual yield.[1, 25]

The patterned substrates both show a small drop in reflection around 40°. To study this in more detail, a high-resolution plot of the two-side patterned substrate, illuminated by s-polarized light, is shown as an inset (Fig. 2b). A strong decrease of 0.7 % absolute in reflection is observed when $\theta > 39.5°$, which is caused by diffraction into guided modes in the substrate. For $8 \leq \theta \leq 39.5°$, the -1 diffraction order can couple to guided modes (see S6 for dispersion calculations and schematic). Light that couples to guided modes couples back out and contributes to the measured reflection amplitude. The dashed line indicates the angle for which the dispersion curve of the diffracted order crosses the light line and beyond which coupling to guided modes no longer occurs. The data shows excellent agreement with the dispersion calculations. Again, coupling to the guided modes will be reduced for encapsulated substrates.

Next, we study the wetting properties of our nanoimprinted coating. Adhesion of water droplets and nucleation of fog on the surface of transparent substrates causes scattering and thereby

increases the overall reflectance. The solgel is more hydrophobic than the bare glass due to the presence of methyl groups. Nanostructuring the surface can further enhance the hydrophobicity, as water droplets partially rest on the nanostructure and partially on air inclusions.[13, 26] Besides a reduction in scattering from water droplets, hydrophobic coatings enhance self-cleaning of the surface as dust particles are picked up and removed by water droplets while rolling off the surface.[13, 27] To quantify the hydrophobicity of our nanopatterned AR coating, 2.5 µL droplets of dH_2O were deposited on bare flat substrates (cleaned with acetone and cleanroom wipe), and substrates coated with flat and patterned solgel layers. Optical microscope images (WiTec α 300 SR) were taken from the side to image the water contact angle.

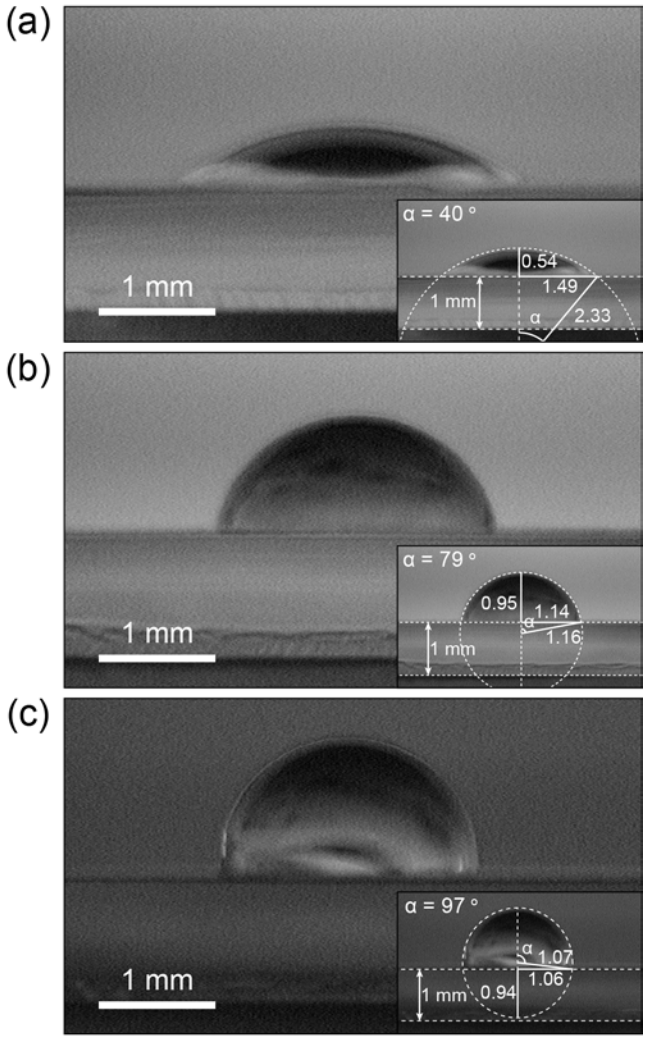

Figure 3. Optical microscope image of dH_2O droplets on a flat reference glass substrate (a), flat solgel layer (b), and nano-patterned solgel layer (c), showing the hydrophobic behavior of the nanopatterned AR coating. From bottom to top, the microscope stage, the glass substrate and the droplet are clearly visible. The geometrical analysis and the calculated contact angles are shown as insets.

The hydrophobicity of the solgel is clearly visible, as the contact angle (Fig. 3b) is much larger than that of a water droplet on the bare flat substrate (Fig. 3a). Indeed, the nanopatterned solgel further increases the water contact angle (Fig. 3c). Geometrical analysis of the droplets shapes (insets) shows contact angles of 40°, 79° and 97° for the bare flat, flat solgel, and patterned

solgel substrates respectively. The contact angle being larger than 90° implies the surface is hydrophobic by definition.[27] Finally, to test the mechanical rigidity of the nanopattern coating we applied, pressed and removed both office tape and vinyl duct tape (3M 3903i) onto the patterned surface. In both cases, the nanopattern was resistant to tape stripping, as no surface modification was observed by SEM imaging (see S7 for details).

The very low reflectance (0.57 % averaged in visible spectral range) and low angle sensitivity (< 1.0 % up to 50°) of the nanopatterned AR coating is comparable to or better than what was obtained with complex graded index moth-eye AR coatings,[10-14] while our fabrication method is much simpler. While the high-aspect ratio of the moth-eye structures is beneficial for hydrophobicity,[10, 13, 14] the reduced aspect ratio of our nanopattern coating makes it much less fragile.

To demonstrate the large-area applicability and ease of fabrication of the AR coating, we printed the nanopattern on the surface of a smart phone screen (Apple iPhone® 4) and compare it to a flat non-patterned screen. Prior to the imprint procedure, the screen was cleaned with isopropanol and a cleanroom wipe. Figure 4a shows a photograph of the reflection of fluorescent ceiling lighting off bare and nano-imprinted screens. A clear reduction in the reflected intensity can be seen from the reduced intensity of the reflected fluorescent lamp. Such reduced reflectance strongly improves the readability of the smartphone screen. The improved contrast between light emitted by the screen and glare from surrounding light (e.g. sun) also reduces the screen brightness that is required for good readability, and can reduce the screen's energy consumption.

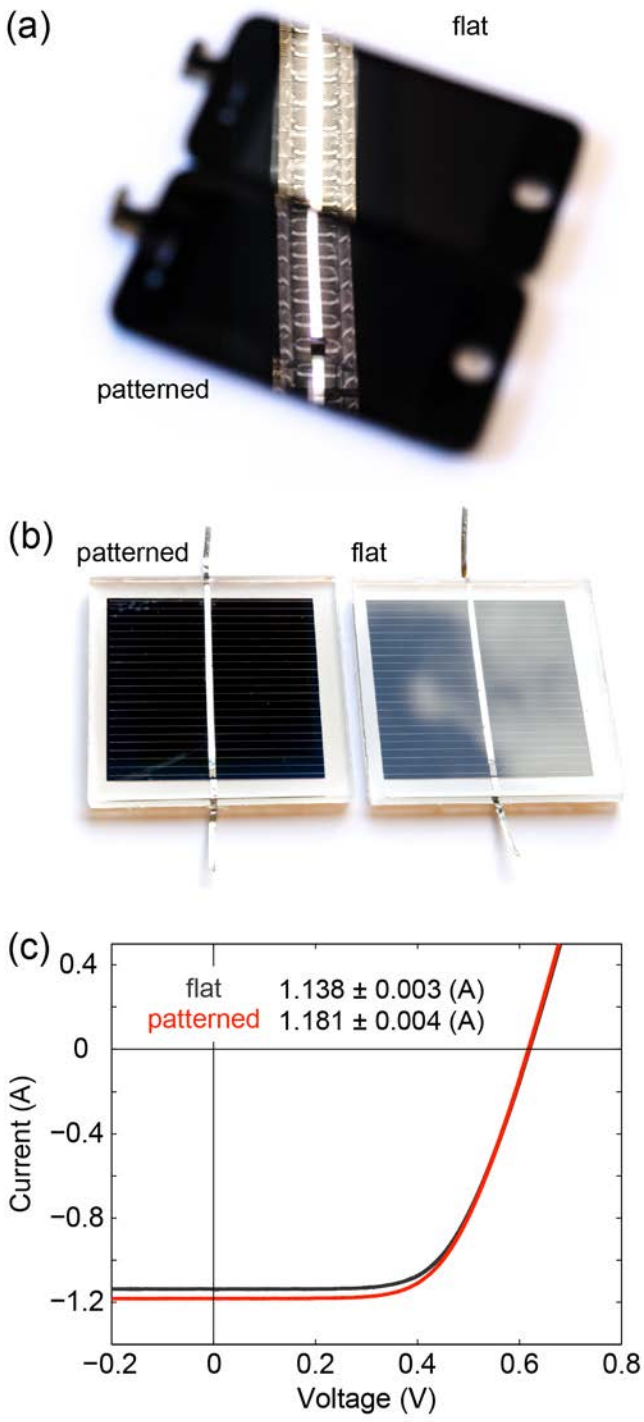

Figure 4. (a) Photograph of smartphone screens with (bottom) and without (top) AR coating. The reflection of the fluorescent lighting is clearly reduced. (b) Photograph of glass-encapsulated c-Si solar cells with (left) and without (right) AR coating. The cell area is 5×5 cm^2. (c) Current-

voltage measurements on the glass-encapsulated solar cells with (red) and without (black) AR coating. The short-circuit current I_{sc} for the two cells is listed: a 3.8 % relative increase is observed due to the AR coating.

To demonstrate the applicability to solar applications, we apply a nanoimprinted AR coating to Si photovoltaic cells encapsulated in glass. We use n-type diffused front-junction c-Si solar cells, which are encapsulated by lamination with a 300 μm thick EVA layer, a 3-mm-thick low-iron glass slide at the front and a white backsheet. The cells were 5×5 cm^2 in size, and framed in a 6×6 cm^2 mini-module. Before patterning the front surface is cleaned with acetone, isopropanol and cleanroom wipes. Figure 4b shows a photograph of the reflection of the clouded outdoor sky off both mini-modules. A clear decrease in reflectance can readily be observed by eye.

To test the influence on cell performance, we measured the current-voltage characteristics of the same cell before and after nanopatterning. A solar simulator (Newport Oriel Sol2A) was used to illuminate the cell with 1.000 ± 0.005 sun intensity. Using a source-measuring unit (Agilent B2902A), the voltage over the cell is scanned from -1.0 to +1.0 V in steps of 2 mV, and the photocurrent is measured. The standard deviation in photocurrent as a result of positioning uncertainties was measured to be < 0.5 %, by repeatedly positioning the cell in the solar simulator and measuring the *I*-*V* response.

Patterning the photovoltaic modules with the nanopatterned AR coating causes the short-circuit current generated by the cell to increase from 1.138 ± 0.003 to 1.181 ± 0.004 A (Fig. 4c). This corresponds to a 3.8 % relative increase in current, increasing the peak output power from 441 to 453 mW. Note that the modules have been measured without masking of the white area around

the cell. Thus, the measured current has a contribution coming from light diffused by the white back sheet and trapped into the glass. This example clearly demonstrates the potential of our nanopattern AR coating for PV applications. The nanopattern applied to both the smart phone screens and photovoltaic modules was the same as that used in Figs. 1-3, and not optimized for the smartphone and solar module glass.

In conclusion, we demonstrate a nano-patterned anti-reflection coating for glass substrates that is fabricated by a simple, single-step silica solgel soft-imprint process. This pattern can be applied to large-areas and can be scaled up to a roll-to-roll process. The imprint-process has very high large-scale uniformity, is substrate conformal, and gives accurate control over effective refractive index and thickness. The pattern made using silica solgel can in theory be optimized for substrates with n = 1.003 – 2.070 by tuning the nanoparticle diameter. Higher indices may be achieved by modifying the solgel composition. We demonstrate that application of the nanopatterned AR coating to both sides of a glass substrate reduces the average reflectance from 7.35 % to 0.59 % in the visible spectral range, with a minimum reflectance < 0.05% at λ = 590 nm. Angle-resolved reflection measurements show < 1.0 % reflectance for the entire angular range up to 50°. We apply the nanopattern anti-reflection coating to smart-phone screens and glass-encapsulated c-Si solar cells. A strong reduction in reflectance can be observed by eye, improving the display visibility in outdoor applications. Photovoltaic modules showed a 3.8 % relative increase in short-circuit current, corresponding to a 2.8 % relative increase in power output. Furthermore, the nanopattern anti-reflection coating makes the surface hydrophobic and can be applied to any type of glass.

ASSOCIATED CONTENT

Supporting Information. Technical information and figures on: ellipsometry data for solgel, total reflection measurement procedures, FDTD simulations, characterization of haze, polarization-resolved reflection spectra, dispersion calculations, and duct tape stripping details. This material is available free of charge via the Internet at http://pubs.acs.org.

AUTHOR INFORMATION

Corresponding Author

*polman@amolf.nl

Author Contributions

The research was initiated by PS, JvdG and AP. JvdG fabricated samples, performed the measurements and analysis. PS provided the photovoltaic modules. JvdG wrote the manuscript, under supervision of AP.

Notes

The authors have applied for a patent on the topic of this paper.

ACKNOWLEDGMENT

The authors gratefully acknowledge Mark Knight for the 3D cartoon in Fig. 1 and photographs in Fig. 4, and Bruno Ehrler for careful reading of the manuscript. The work at AMOLF is part of the research program of the “Stichting voor Fundamenteel Onderzoek der Materie (FOM)”, which is financially supported by the “Nederlandse Organisatie voor Wetenschappelijk Onderzoek (NWO)”. It is also supported by the European Research Council and NanoNextNL, a research and technology program of the Dutch ministry of Economic Affairs.

REFERENCES

1. Ballif, C.; Dicker, J.; Borchert, D.; Hofmann, T. *Sol. Energy Mater. Sol. Cells* **2004,** *82*, 331-344.

2. Cid, M.; Stem, N.; Brunetti, C.; Beloto, A. F.; Ramos, C. A. S. *Surf. Coat. Technol.* **1998,** *106*, 117-120.

3. Li, H. H. *J. Phys. Chem. Ref. Data* **1980,** *9*, 161-290.

4. Chen, D. *Sol. Energy Mater. Sol. Cells* **2001,** *68*, 313-336.

5. Uhlmann, D. R.; Suratwala, T.; Davidson, K.; Boulton, J. M.; Teowee, G. *J. Non-Cryst. Solids* **1997,** *218*, 113-122.

6. Aben, G.; Kockelkorel, T.; Li, Y.; Matloka, K.; Plaum, M.; de Rijk, R.; Schoot, H.; Voicu, N., Light transmittance enhancement over lifetime performance of anti-reflective PV module cover glass. http://www.dsm.com/corporate/markets-products/markets/energy/khepricoat.html (accessed April 14, 2015).

7. Yoldas, B. E.; Partlow, D. P. *Appl. Opt.* **1984,** *23*, 1418-1424.

8. Wang, K. X.; Yu, Z.; Sandhu, S.; Liu, V.; Fan, S. *Optica* **2014,** *1*, 388-395.

9. Spinelli, P.; Verschuuren, M. A.; Polman, A. *Nat Commun* **2012,** *3*, 692.

10. Han, K.-S.; Shin, J.-H.; Lee, H. *Sol. Energy Mater. Sol. Cells* **2010,** *94*, 583-587.

11. Hong, S.-H.; Bae, B.-J.; Han, K.-S.; Hong, E.-J.; Lee, H.; Choi, K.-W. *Electron. Mater. Lett.* **2009,** *5*, 39-42.

12. Deniz, H.; Khudiyev, T.; Buyukserin, F.; Bayindir, M. *Appl. Phys. Lett.* **2011,** *99*, 183107.

13. Park, K.-C.; Choi, H. J.; Chang, C.-H.; Cohen, R. E.; McKinley, G. H.; Barbastathis, G. *ACS Nano* **2012,** *6*, 3789-3799.

14. Raut, H. K.; Dinachali, S. S.; Loke, Y. C.; Ganesan, R.; Ansah-Antwi, K. K.; Góra, A.; Khoo, E. H.; Ganesh, V. A.; Saifullah, M. S. M.; Ramakrishna, S. *ACS Nano* **2015,** *9*, 1305-1314.

15. Min, W.-L.; Jiang, B.; Jiang, P. *Adv. Mater.* **2008,** *20*, 3914-3918.

16. Askar, K.; Phillips, B. M.; Fang, Y.; Choi, B.; Gozubenli, N.; Jiang, P.; Jiang, B. *Colloids and Surfaces A: Physicochemical and Engineering Aspects* **2013,** *439*, 84-100.

17. Hattori, H. *Adv. Mater.* **2001,** *13*, 51-54.

18. Szczyrbowski, J.; Bräuer, G.; Teschner, G.; Zmelty, A. *J. Non-Cryst. Solids* **1997,** *218*, 25-29.

19. Jeasung, S. Study of nanostructured glass surfaces for photovoltaic applications. Ph.D Thesis, National University of Singapore, August 2013.

20. Verschuuren, M. A. Substrate Conformal Imprint Lithography for Nanophotonics. Ph.D Thesis, Utrecht University, March 2010.

21. Sharpe, L. T.; Stockman, A.; Jagla, W.; Jägle, H. *Journal of Vision* **2005,** *5*, 948-968.

22. Stavenga, D. G.; Foletti, S.; Palasantzas, G.; Arikawa, K. *Proceedings of the Royal Society B: Biological Sciences* **2006,** *273*, 661-667.

23. Maxwell Garnett, J. C. *Philosophical Transactions of the Royal Society of London. Series A* **1904,** *203*, 385-420.

24. Bruggeman, D. A. G. *Annalen der Physik* **1935,** *416*, 636-664.

25. Fatehi, J. H.; Sauer, K. J. In *Modeling the incidence angle dependence of photovoltaic modules in PVsyst*, Photovoltaic Specialist Conference (PVSC), 2014 IEEE 40th, 8-13 June 2014, 2014; pp 1335-1338.

26. Cassie, A. B. D.; Baxter, S. *Trans. Faraday Society* **1944,** *40*, 546-551.

27. Forbes, P. *Sci. Am.* **2008,** *299*, 88-95.

Table of Contents Graphic